

Self-assembly of binary solutions to complex structures

Alberto Scacchi,^{1,2,*} Maria Sammalkorpi,^{1,3} and Tapio Ala-Nissilä^{4,5}

¹*Department of Chemistry and Materials Science,
Aalto University, P.O. Box 16100, FI-00076 Aalto, Finland*

²*Department of Applied Physics, Aalto University, P.O. Box 11000, FI-00076 Aalto, Finland*

³*Department of Bioproducts and Biosystems, Aalto University, P.O. Box 16100, FI-00076 Aalto, Finland*

⁴*Quantum Technology Finland Center of Excellence and Department of Applied Physics,
Aalto University, P.O. Box 11000, FI-00076 Aalto, Finland*

⁵*Interdisciplinary Centre for Mathematical Modelling and Department of Mathematical Sciences,
Loughborough University, Loughborough, Leicestershire LE11 3TU, United Kingdom*

(Dated: March 1, 2025)

Self-assembly in natural and synthetic molecular systems can create complex aggregates or materials whose properties and functionality rises from their internal structure and molecular arrangement. The key microscopic features that control such assemblies remain poorly understood, nevertheless. Using classical density functional theory we demonstrate how the intrinsic length scales and their interplay in terms of interspecies molecular interactions can be used to tune soft matter self-assembly. We apply our strategy to two different soft binary mixtures to create guidelines for tuning intermolecular interactions that lead to transitions from fully miscible, liquid-like uniform state to formation of simple and core-shell aggregates, and mixed aggregate structures. Furthermore, we demonstrate how the interspecies interactions and system composition can be used to control concentration gradients of component species within these assemblies. The insight generated by this work contributes towards understanding and controlling soft multi-component self-assembly systems. Additionally, our results aid in understanding complex biological assemblies and their function and provide tools to engineer molecular interactions in order to control polymeric and protein-based materials, pharmaceutical formulations, and nanoparticle assemblies.

I. INTRODUCTION

In self-assembly of molecular systems, a disordered solution spontaneously organizes to form ordered structures or assembly patterns from its components. Examples of natural and synthetic materials where self-assembly, the resulting complex structures, and their advanced functional properties are central [1] include molecular crystals [2, 3], colloids [4], lipid membranes [5], polymer assemblies [6–8], self-assembled monolayers [9, 10] and quasicrystalline structures [11]. Basic biological cell function relies on self-assembly phenomena such as spontaneous condensation [12] or lipid raft formation [13]. Also technologically, self-assembling soft materials are receiving a great deal of attention in a variety of applications including drug delivery [14–16] and anticancer therapy [17, 18], nanotechnology photonics [2, 19–21], polymer [20, 21] and other electronics [22], as well as biointerfaces and bioengineering [23, 24].

At the level of thermodynamics the properties of molecular self-assemblies in surfactant, biomolecular, and polymer solutions, such as micellization, emulsion formation, or self-assembling monolayers and bilayers can be explained at the level of interplay between water entropy, the relevant surface tensions and corresponding free energies [25–27]. However, understanding self-assembly systems involving multiple components, especially the mechanisms giving rise to the complex assembly characteris-

tics in them, requires more advanced theoretical efforts. To this end, in this manuscript, we present a general theoretical framework based on classical density functional theory (DFT) [28–30] demonstrating how competition between molecular interactions can lead to molecular solutions transitioning from simple uniform mixtures or particle formation to spontaneous ordering to structurally complex assemblies such as core-shell molecular assemblies (micelles or polymer particles) and assemblies with internal molecular composition gradients or layering. Such assemblies are widely present in surfactant and biosystems (micelles, vesicles, emulsion type formulations, biomolecular droplets) [12, 31, 32] but also readily formed by polymer assemblies [6–8, 21]. Understanding the spontaneous assembly transitions and controlling the composition gradients, for example, hydrophobic-hydrophilic gradients, is particularly important for designing solubilization and partitioning systems e.g. for separation and extraction [33] or drug delivery systems [34–37]. The self-assembling micro-environments also form synthetic biology artificial cells [38, 39] and confined catalysis systems [40, 41].

In DFT, free-energy potentials are used to model interactions between the species in the system. This enables extracting an inhomogeneous average density of the different components in the thermodynamic equilibrium based on energy minimization principles [28–30]. In the last few years, DFT has been successfully applied to multi-component systems to describe various other forms of self-assembly, such as superlattice structures [42], quasicrystals [43–45] and general multiple length scale self-assembly [46]. In this approach, the linear dispersion

* alberto.scacchi@aalto.fi

relation [43, 47–51] provides the key quantity used to provide guidelines to generate appropriate interparticle potentials. The importance of the linear dispersion relation in constructing the effective interactions is also emphasized by its recent application to accurately capture non-equilibrium phenomena such as laning instability [52] and to control the macroscopic structures of systems under external shear [53].

II. THEORY

Using DFT, we can obtain the equilibrium average density distribution of a binary mixture suspended in a (implicit) background fluid. In other words, our model captures the interactions of regions of two different chemical characteristics in a solution to predict how molecular species, corresponding to those chemical characteristics, would assemble and organize. Although these interaction characteristics emerge from the molecular level, we emphasize that the "particles" in our model implicitly include interaction effects from their solution environment, as well.

The total grand potential of a system composed by two distinct types of particles is described by

$$\Omega[\rho_1, \rho_2] = \mathcal{F}[\rho_1, \rho_2] + \sum_{i=1,2} \int d\mathbf{r} [V_i^{\text{ext}}(\mathbf{r}) - \mu_i] \rho_i(\mathbf{r}), \quad (1)$$

where \mathcal{F} is the intrinsic Helmholtz free energy functional, $V_i^{\text{ext}}(\mathbf{r})$ is the one-body external potential acting on species i , μ_i the corresponding chemical potential and $\rho_i(\mathbf{r})$ the average (inhomogeneous) one body number density. The intrinsic Helmholtz free energy can be written as

$$\mathcal{F}[\rho_1, \rho_2] = \mathcal{F}^{\text{id}}[\rho_1, \rho_2] + \mathcal{F}^{\text{exc}}[\rho_1, \rho_2], \quad (2)$$

where the first term is the ideal gas contribution. The latter functional has the known form

$$\mathcal{F}^{\text{id}}[\rho_1, \rho_2] = k_B T \sum_{i=1,2} \int d\mathbf{r} \rho_i(\mathbf{r}) [\ln(\Lambda_i^d \rho_i(\mathbf{r})) - 1], \quad (3)$$

where Λ_i is the thermal de Broglie wavelength and d is the dimensionality of the system (here we focus on $d = 2$ for simplicity, but our findings are expected to be valid in $d = 3$ as well, where additional configurations are to be expected). The second term in Eq. (2) is the excess Helmholtz free energy functional, which describes the interactions between the particles. Following Ramakrishnan and Yussouff [54], we opt for an expansion of the latter functional around the homogeneous fluid states ρ_i^0 , $i = 1, 2$, in a functional Taylor expansion and truncate

at second order, leaving us with

$$\begin{aligned} \mathcal{F}^{\text{exc}}[\rho_1, \rho_2] &= \mathcal{F}^{\text{exc}}[\rho_1^0, \rho_2^0] + \sum_{i=1,2} \int d\mathbf{r} \mu_i^{\text{ex}} \delta\rho_i(\mathbf{r}) \\ &\quad - \frac{1}{2\beta} \sum_{\substack{i=1,2 \\ j=1,2}} \int d\mathbf{r} \int d\mathbf{r}' \delta\rho_i(\mathbf{r}) c_{ij}(|\mathbf{r} - \mathbf{r}'|) \delta\rho_j(\mathbf{r}'), \end{aligned} \quad (4)$$

where $\delta\rho_i(\mathbf{r}) = \rho_i(\mathbf{r}) - \rho_i^0$ and $\mu_i^{\text{ex}} = \mu_i - k_B T \ln(\rho_i^0 \Lambda_i)$ are the excess chemical potential, $c_{ij}(\mathbf{r})$ are the direct correlation functions, and $\beta = 1/k_B T$. There are different ways to approximate the latter functions. The choice of the approximation depends on the type of interactions that one considers for the model. For this study, we choose the random phase approximation (RPA), which corresponds to $c_{ij}(\mathbf{r}) = -\beta\phi_{ij}(\mathbf{r})$, where $\phi_{ij}(\mathbf{r})$ are effective pair potentials [55]. This approximation has proven to be very efficient when dealing with soft interactions in polymer, surfactant, and other macromolecular systems including dendrimers or star polymers [46, 56–59], and even for describing structure and dynamics of cells in living tissues and tumors [60]. However, if more accurate approximations were needed, one could for example use the so-called hypernetted chain (HNC) Ornstein-Zernike integral equation theory [28] to obtain the direct correlation functions $c_{ij}(\mathbf{r})$ in Eq. (4). Such approach has recently been applied to e.g. describe nanoparticles forming quasicrystals [44].

The equilibrium average density profiles $\rho_i(\mathbf{r})$ are those which minimise the functional of the grand potential $\Omega[\rho_1, \rho_2]$. Therefore, they also satisfy the coupled Euler-Lagrange equations

$$\frac{\delta\Omega[\rho_1, \rho_2]}{\delta\rho_i} = 0, \quad (5)$$

for $i = 1, 2$. For bulk systems, i.e. for $V_i^{\text{ext}}(\mathbf{r}) \equiv 0$ for $i = 1, 2$ in Eq. (1), this is equivalent to solving the following coupled equations for $\rho_1(\mathbf{r})$ and $\rho_2(\mathbf{r})$

$$\ln\left(\frac{\rho_i(\mathbf{r})}{\rho_i^0}\right) - \beta \sum_{j=1,2} \int d\mathbf{r}' c_{ij}(|\mathbf{r} - \mathbf{r}'|) \delta\rho_j(\mathbf{r}') = 0. \quad (6)$$

The results presented hereafter are obtained solving Eq. (6) under periodic boundary conditions.

A. The dispersion relation

The two branches of the dispersion relation for a binary (isotropic) mixture are [50]

$$\omega_{\pm}(k) = \frac{1}{2} \text{Tr}(\mathbf{ME}) \pm \sqrt{\frac{1}{4} \text{Tr}(\mathbf{ME})^2 - \det(\mathbf{ME})}, \quad (7)$$

where the two matrices \mathbf{M} and \mathbf{E} are defined as

$$\mathbf{M} = -k^2 \begin{pmatrix} D_1 \rho_1^0 & 0 \\ 0 & D_2 \rho_2^0 \end{pmatrix}, \quad (8)$$

and

$$\mathbf{E} = \begin{pmatrix} \left[\frac{1}{\rho_1^0} - \hat{c}_{11}(k) \right] & -\hat{c}_{12}(k) \\ -\hat{c}_{21}(k) & \left[\frac{1}{\rho_2^0} - \hat{c}_{22}(k) \right] \end{pmatrix}, \quad (9)$$

respectively. In these, $\hat{c}_{ij}(k)$ are the Fourier transform of the direct correlation functions $c_{ij}(r)$ and D_i is the diffusion coefficient of species i . If $\omega_{\pm} < 0$, for all wave numbers $k = |\mathbf{k}|$, $k \in \mathbb{R}$, then all k modes decay and the uniform state is linearly stable. It is easy to see that $\omega_-(k) \leq \omega_+(k)$. Thus, if $\omega_+ > 0$ for some values of k , then such modes grow over time and will dominate the density modulation of the system.

It is worth mentioning that the values of the diffusion coefficients D_1 and D_2 do not influence the thermodynamic equilibrium state, i.e. the minimum of the free energy, and therefore, are not involved further.

B. The Ornstein-Zernike equation for binary mixtures

The total correlation functions $h_{ij}(r)$, which are related to the radial distribution functions $g_{ij}(r)$ via $h_{ij}(r) = g_{ij}(r) - 1$, can be obtained using the Ornstein-Zernike (OZ) equations. For a binary (isotropic) fluid mixture, the OZ equations are [28]:

$$h_{ij}(r) = c_{ij}(r) + \sum_{k=1,2} \rho_k^0 \int d\mathbf{r}' c_{ik}(|\mathbf{r} - \mathbf{r}'|) h_{kj}(r'). \quad (10)$$

These coupled equations must be solved in conjunction with the (exact) closure relations

$$c_{ij}(r) = -\beta \phi_{ij}(r) + h_{ij}(r) - \ln[1 + h_{ij}(r)] + B_{ij}(r), \quad (11)$$

where $B_{ij}(r)$ are the so-called bridge functions [28]. For example, the HNC approximation consists of setting $B_{ij}(r) = 0 \forall r$. The RPA approximation can be obtained by linearising the logarithm in Eq. (11) together with the HNC approximation. It is also worth mentioning that when modelling strongly repulsive and short-range interactions, the direct correlation functions can be obtained employing the Percus-Yevick approximation [28].

C. The partial static structure factors

The partial static structure factors, which are accessible via scattering experiments, are defined as [28, 50]:

$$\begin{aligned} S_{11}(k) &= 1 + \rho_1^0 \hat{h}_{11}(k); \\ S_{22}(k) &= 1 + \rho_2^0 \hat{h}_{22}(k); \\ S_{12}(k) &= \sqrt{\rho_1^0 \rho_2^0} \hat{h}_{12}(k), \end{aligned} \quad (12)$$

where the Fourier transform of the total correlation functions \hat{h}_{ij} are

$$\hat{h}_{ij}(k) = \frac{N_{ij}(k)}{D(k)}, \quad (13)$$

with the numerators $N_{ij}(k)$ given by

$$\begin{aligned} N_{11}(k) &= \hat{c}_{11}(k) + \rho_2^0 [\hat{c}_{12}^2(k) - \hat{c}_{11}(k)\hat{c}_{22}(k)]; \\ N_{22}(k) &= \hat{c}_{22}(k) + \rho_1^0 [\hat{c}_{12}^2(k) - \hat{c}_{11}(k)\hat{c}_{22}(k)]; \\ N_{12}(k) &= \hat{c}_{12}(k), \end{aligned} \quad (14)$$

and the common denominator

$$D(k) \equiv [1 - \rho_1^0 \hat{c}_{11}(k)] [1 - \rho_2^0 \hat{c}_{22}(k)] - \rho_1^0 \rho_2^0 \hat{c}_{12}^2(k). \quad (15)$$

In the case of a stable liquid, $D(k) > 0 \forall k$. Otherwise, the liquid state is linearly unstable. This enables determining the stability threshold, or the instability onset, for the uniform liquid from solving for the locus in the phase diagram where a solution to the equation $D(k) = 0$ appears.

III. MODEL FOR CORE-SHELL ASSEMBLIES

For computational efficiency, we focus here on a two-dimensional (2D) model. In order to study a model for a binary mixture that can be expected to form assemblies in which an internal core is surrounded by a corona shell differing in composition, both from the core and the bulk solution, we model the effective interactions of the different components as

$$\begin{aligned} \phi_{11}(r) &= \varepsilon_{11} e^{-(r/R_{11})^4}; \\ \phi_{12}(r) &= \varepsilon_{12}^- e^{-(r/R_{12}^-)^2} + \varepsilon_{12}^+ e^{-(r/R_{12}^+)^2}; \\ \phi_{22}(r) &= \varepsilon_{22} e^{-(r/R_{22})^2}, \end{aligned} \quad (16)$$

where $\beta\varepsilon_{12}^- < 0$ and $\beta\varepsilon_{12}^+ > 0$, with the constraint $|\beta\varepsilon_{12}^-| < |\beta\varepsilon_{12}^+|$. Additionally, $R_{12}^- > R_{12}^+$. Together, these design a short ranged repulsion and a long ranged attraction between the two species. The different variables chosen in this work for this model are reported in Table I. Note that for the cross-interaction, the inte-

$\beta\varepsilon_{11}$	$\beta\varepsilon_{12}^-$	$\beta\varepsilon_{12}^+$	$\beta\varepsilon_{22}$	R_{11}	R_{12}^-	R_{12}^+	R_{22}
1	-1	25	1	1	0.5	0.1	1

TABLE I. Set of dimensionless parameters used in Eq. (16) to model core-shell particles.

grated strength $2\pi \int_0^\infty r \phi_{12}(r) dr = 0$. The different potentials in Eq. (16) have been chosen following the fact that in order to see the formation of clusters of purely repulsive particles, one needs in the model an intrinsic length scale that can eventually be unstable. Such property implies a symmetry breaking, and thus the formation of periodic (or aperiodic) patterns. In the current work, the interaction between particles of species 1 bear such a feature and is modelled using the so-called generalised exponential model of order n (GEM- n) [48, 49, 61–69]. Here $n = 4$. In order to keep the model as simple as possible, species 2 is modelled using the Gaussian core

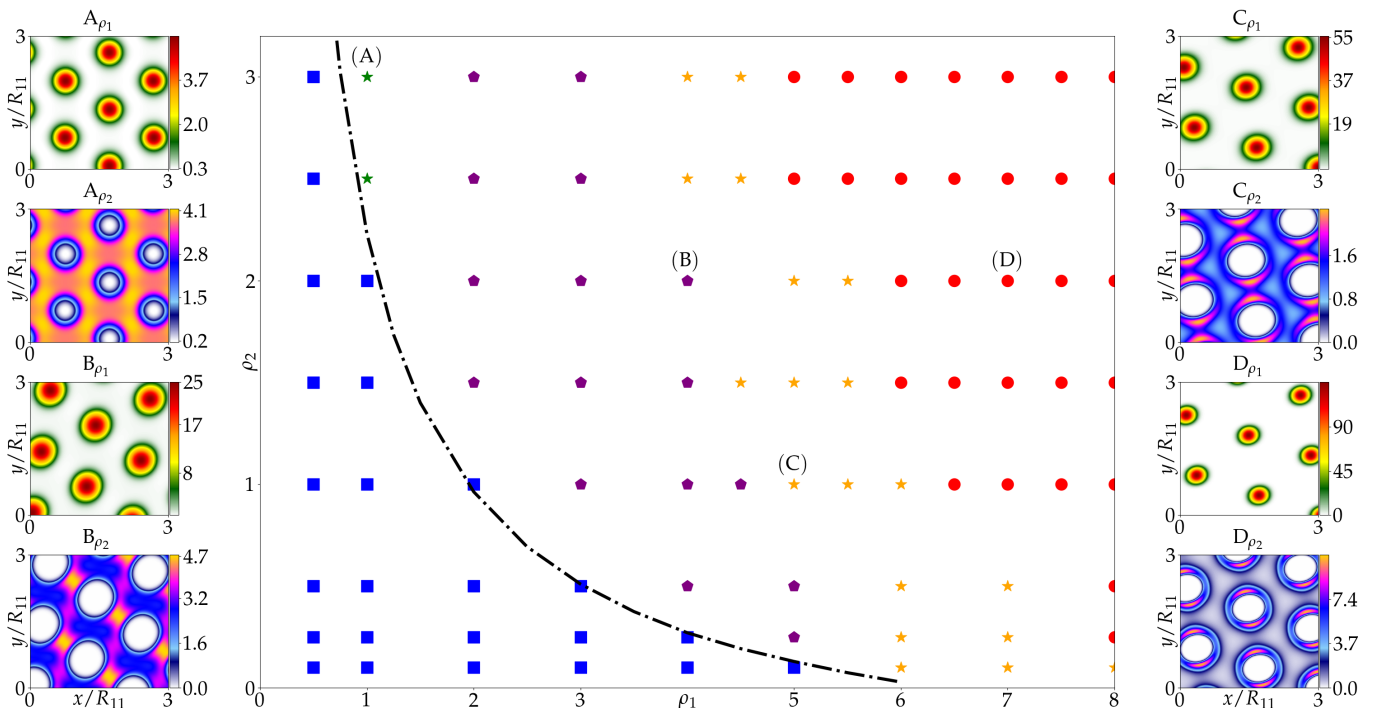


FIG. 1. Phase diagram of the different states in the (ρ_1^0, ρ_2^0) plane corresponding to the model of Eq. (16) and parameters in Table I. Letter labels identify the side panel visualizations for ρ_1 and ρ_2 at the identified state point, respectively. Blue squares represent homogeneous states (both species in the liquid state, mixing uniformly). Green stars represent states where species 1 assembles in higher average density domains that follow hexagonal assembly structure and species 2 remains liquid-like uniformly avoiding the latter peaks (see panels A_{ρ_1} and A_{ρ_2} , for ρ_1 and ρ_2 distribution examples). Purple pentagons represent states in which species 1 condense with a hexagonal pattern and species 2 avoids the latter sites, not as a uniform liquid but with some underlying lattice structure in its density distribution. However, the species 2 layer surrounding the sites occupied by species 1 has a lower particle density than that of the bulk mean density (see panels B_{ρ_1} and B_{ρ_2}). The orange stars represent states in which species 1 condenses to hexagonally distributed sites and species 2 assembles around the latter sites. Away from ρ_1 peaks, the distribution of species 2 is almost liquid-like, but with a residual underlying structure (see panels C_{ρ_1} and C_{ρ_2}). Red disks represent states where species 1 peaks form hexagons and species 2 strongly gathers around the ρ_1 peaks. Practically all ρ_1 and ρ_2 gather into these sites leaving the rest of the system relatively empty, or dilute (see panels D_{ρ_1} and D_{ρ_2} for an example). The linear instability line is shown by the dash-dotted line.

model (GCM), which does not belong to the class of $Q\pm$ -interactions [70], i.e. it does not lead to cluster formation in single-component mixtures (except for $\varepsilon\beta > 100$ [56], irrelevant here). The GCM has been extensively used to model polymeric interactions [55, 65, 71–77]. The second term in the cross-interaction ϕ_{12} models a short range repulsion, which is necessary to avoid overlap of particles of different species. However, in order to favor the formation of a shell surrounding the core of the particle, attraction between different species is also necessary. The latter is achieved via the first term in ϕ_{12} . It is worth mentioning that the results presented here are expected to be valid for a variety of interaction potentials which bear properties similar to those in the current model, Eq. (16). The results can also be expected to hold for a large collection of parameters different from those reported in Table I.

A. Results

We explore the density density plane (ρ_1^0, ρ_2^0) to resolve the equilibrium self-assembly phases adopted by a system following the interaction parameters reported in Table I. Here ρ_1^0 and ρ_2^0 are the bulk number densities of species 1 and species 2, respectively. The resulting assembly phase diagram and the four different assembly configurations adopted by the system in different composition regions are shown in Fig. 1. For each state point, we report the density of both species 1 and species 2, labelled accordingly. The phase diagram indicates that the system adopts a homogenous mixture corresponding to uniform solution of species 1 and 2 at low concentrations of ρ_1 (blue squares) while an increase of ρ_1 leads to an onset of species 1 condensation into islands that exhibit hexagonal symmetry. This occurs at a concentration that is dependent on ρ_2^0 . The data of Figure 1 indicates that the system has only one phase transition. The transition happens when passing from the homoge-

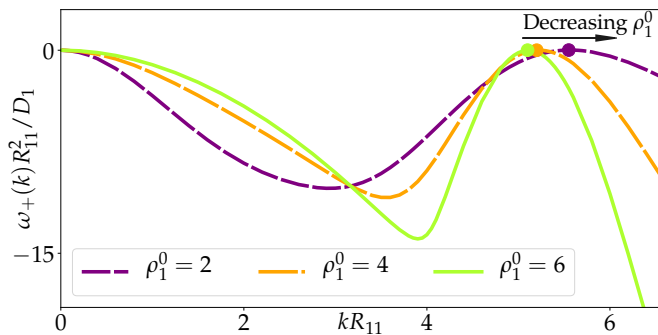


FIG. 2. Different onsets of the linear instability, i.e. the marginal condition for density modulation in the system, as a function of ρ_1^0 (dash-dotted line in the central panel of Fig. 1). The critical wave numbers k_c , marked by circles, shift to higher values as ρ_1^0 decreases, which corresponds to the lattice constant of the expected periodic structure decreasing. Additionally, the peaks in the dispersion relations broaden as the bulk density of species 1 decreases. This indicates the selectivity of the wave number k_c softens.

neous state (blue squares) to any state with hexagonal symmetry in species 1 assembly pattern. The presence of a single phase transition is expected, since the system has only one intrinsic length scale.

While species 1 assembles into condensation islands with hexagonal symmetry in spatial locations throughout the structure forming part of the phase diagram, species 2 shows interesting configurational changes when exploring different concentrations. In the first two of these, species 2 adopts a distribution where it avoids the locations where species 1 is enriched as clusters. A region with very low density, i.e. a depletion region of ρ_2 is formed around the ρ_1 islands. In the green stars states of Figure 1, most of ρ_2 forms a uniform background solution with density very close to the bulk value ρ_2^0 in the regions where ρ_1 is absent. An example of this configuration is shown in Fig. 1, panels A_{ρ_1} and A_{ρ_2} . Such assembly corresponds to, for example, multicomponent polymer solutions in which one species forms polymer particles and another remains soluble, yet immiscible with the former species. One can consider this also as two immiscible liquids, with ρ_1 forming droplets surrounded by the phase in which ρ_2 spreads uniformly to form a continuous phase. Such phase separation occurs, for example in intracellular liquid-liquid phase separation or coacervation of macromolecule solutions.

In the states marked by purple pentagons, similar holes in ρ_2 around the ρ_1 condensation sites characterize the density distribution. However, ρ_2 distribution shows an underlying periodic structure in the regions where particles 2 are in the liquid state (see panels B_{ρ_1} and B_{ρ_2} of Fig. 1). This represents species 1 driving correlations into the structure formation of species 2, despite species 2 retaining partial liquid character. Transition from the uniform background species 2 to this correlated species 2 distribution is an indication of increasing effective at-

traction between the assembled species 1 islands via the species 2 condensation. This would show in practical systems as increasing solution viscosity.

The orange stars state points correspond to configurations in which species 2 gather around the peaks of ρ_1 defining the primary hexagonal structure. Away from these condensation islands however, the density of both ρ_1 and ρ_2 is depleted. These state points correspond to a partial (or soft) encapsulation of species 1 by a coating of species 2. An example of the latter configuration is shown in Fig. 1, panels C_{ρ_1} and C_{ρ_2} . Such assembly occurs, for example, in amphiphile mediated solubilization or dispersion under conditions where part of the coating species remains soluble. This assembly also corresponds to part of the species 2 assembling into micellar or core-shell particles, part remaining soluble.

Finally, the red disks correspond to structures where species 2 surrounds (almost) completely the clusters of species 1. This leads to a strong encapsulation configuration corresponding to micellar or core-shell type well-defined layered self-assembly structures in e.g. surfactant and polymer systems. This configuration is shown in panels D_{ρ_1} and D_{ρ_2} of Fig. 1. The asymmetry in the shells is a result of the relatively strong and long-ranged repulsion between particles of species 2 via $\phi_{22}(r)$. The asymmetry can be reduced by diminishing the strength and range of this repulsion (see Appendix). The instability line obtained from the dispersion relation $\omega_{\pm}(k)$ is reported in the central panel of Fig. 1. Left of this line the system is expected to be linearly stable which leads to the equilibrium density distribution being homogeneous. At right of this line, however, the system is expected to form patterns with lattice spacing corresponding to $\approx 2\pi/k_c$. Here k_c is the wave number at which the system is marginally unstable. This corresponds to $\omega_+(k_c) = 0$ and $d\omega_+(k_c)/dk = 0$. Careful examination of the critical wave number k_c value for different pairs of bulk densities ρ_1^0 and ρ_2^0 reveals a monotonic shift such that moving along the instability line from high to low values of ρ_1^0 , k_c increases. This means also that the lattice constant of the underlying hexagonal structure decreases. Additionally, the peak in the dispersion relation broadens, which translates into a less selective instability. The latter result is reported in Fig. 2.

It is worth mentioning that at temperatures relevant here, two dimensional monodisperse systems with only hexagonal structures of lattice spacing $\approx R_{11}$, i.e. approximately constant lattice spacing for all densities, are expected [59]. However, this is not true in three dimensions, where a series of isostructural phase transitions are expected at low temperatures [78, 79].

IV. MODEL FOR MIXED PARTICLES

Exchanging the short ranged repulsion and the long-ranged attraction with a short-ranged attraction and a long ranged repulsion, enables obtaining density distri-

butions which are commensurate with mixed assembled particles. This means $\beta\varepsilon_{12}^- < 0$, $\beta\varepsilon_{12}^+ > 0$, with the constraint $|\beta\varepsilon_{12}^-| > |\beta\varepsilon_{12}^+|$, and also $R_{12}^- < R_{12}^+$. Following Section III, the effective pair potentials used in this model are described by Eq. (16), however, the coefficients differ from Sec. III and are reported in Table II. To control the size and composition of the particles we vary the range of the attractive and repulsive contributions in ϕ_{12} , i.e. R_{12}^- and R_{12}^+ , respectively, keeping $R_{12}^- < R_{12}^+$. Note that the integrated strength of the cross-interaction is positive for all five cases discussed here, i.e. $2\pi \int_0^\infty r\phi_{12}(r)dr > 0$.

$\beta\varepsilon_{11}$	$\beta\varepsilon_{12}^-$	$\beta\varepsilon_{12}^+$	$\beta\varepsilon_{22}$	R_{11}	R_{22}
1	-1	0.5	1	1	1

TABLE II. Set of dimensionless parameters used in Eq. (16) to model mixed particles.

A. Results

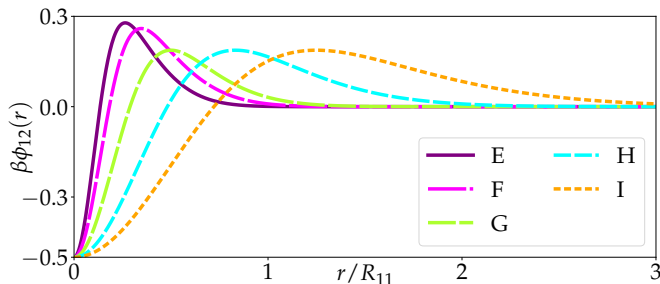


FIG. 3. Cross-interaction potentials ϕ_{12} following the parameters reported in Table II for varying values of R_{12}^- and R_{12}^+ in Table III.

We set the average densities of the two components of the system to $\rho_1^0 R_{11}^2 = 6.5$ and $\rho_2^0 R_{22}^2 = 3$, respectively, and study the equilibrium configurations obtained using the DFT described in Section II as a function of different cross interaction potentials. The form of the inter-species

Model	E	F	G	H	I
R_{12}^-	0.15	0.2	0.3	0.5	0.75
R_{12}^+	0.4	0.5	0.6	1	1.5

TABLE III. Range of the attractive and repulsive contribution in the cross particles interaction potential $\phi_{12}(r)$ leading to mixed particles with different density gradients.

interaction potentials described by the parameters in Table III are shown in Fig. 3.

Figure 4 shows the resulting equilibrium density distributions of both species with species 1 as the top row and species 2 as the bottom row. As before, species 1 assembles into condensation islands with hexagonal spacing throughout the examined parameter range. Only minor changes in condensation peak distribution height and

width can be observed. However, rather interesting assembly changes occur to species 2. In case E, the very short attraction causes a relatively small increment of ρ_2 around the locations occupied by species 1. The repulsive part of ϕ_{12} however causes a depleted region around the latter peaks. Here ρ_2 forms a thin, skin-like, layer around the species 1 condensation island and is separated from bulk by a depletion region. Beyond the depletion region, species 2 adopt an almost liquid-like assembly but showing preferred density locations as triangles formed between the ρ_1 neighboring peaks. This assembly pattern means that also for the species 2, hexagonal order with lattice parameter differing from that of species 1 ordering emerges.

In case F, the total attraction strength between the two components is increased. The attraction is strong enough to pull almost all species 2 particles to the sites enriched in species 1. The clusters of species 2 are very narrow for this set of parameters, and actually now species 1 forms the coating layer. However, no clear core phase exists and the two species remain mixed in the island center regions, however with strong concentration gradients. A low density honeycomb-like region of ρ_2 is visible far from these condensation peaks indicating some of species 2 remaining soluble outside species 1 islands.

Similar to case F, also in setup G, ρ_2 exhibits sharp and narrow peaks at the locations of particles 1. The width of the ρ_2 peaks is practically the same as those of ρ_1 . This means that both species occupy the same region and readily mix. Moving to cases H and I, the widths of both ρ_1 and ρ_2 peaks increase. Eventually, the peaks of ρ_2 become larger than those of species 1 leading to a case where species 1 can be found mostly in the centre of the particles. Even in this case I, also ρ_2 is enriched at the same location meaning that both density and condensation have a gradient in the island.

To summarize the assembly findings, Figure 5 shows the 1D density profiles of the islands for states F, H and I. The data are normalised by the maximal values of the distributions and centered at the maximum of the peak. The figure visualizes how to control the size of the mixed particles, as well as guidelines to engineering the density gradient of the two species mixing inside the particle, but also the overall particle density profile. At a practical level, such concentration gradients mean variations in the local chemical environment. This has a major significance for applications. For example, hydrophilicity-hydrophobicity gradients control drug species partitioning into carrier species and density differences in-out diffusion, for example release of carried species.

V. SUMMARY AND CONCLUSIONS

Using classical density functional theory, we have presented a general framework demonstrating how competition between molecular interactions can lead to the spontaneous formation of structurally complex self-assembly

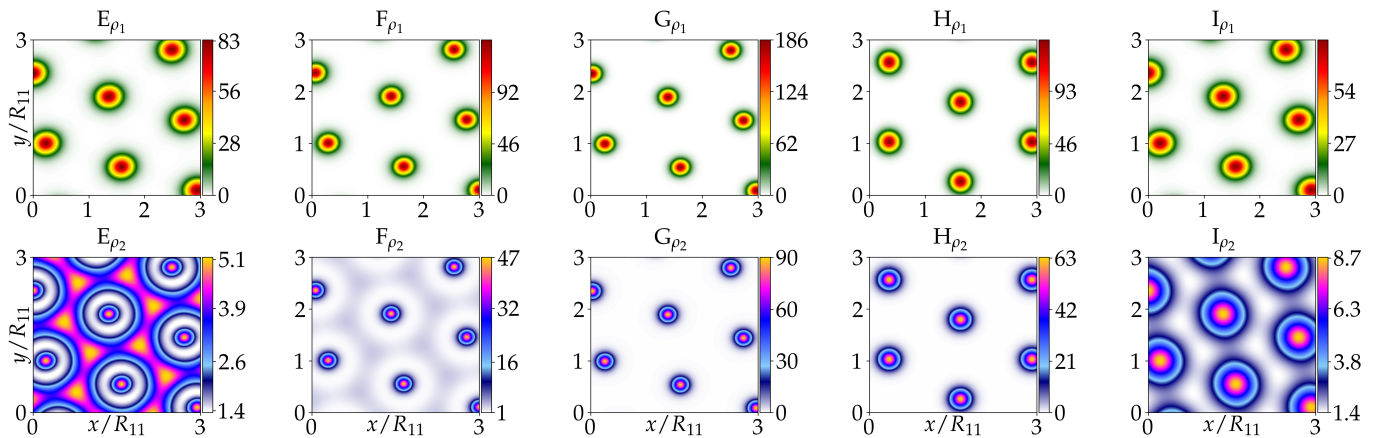


FIG. 4. Average density distribution of species 1 (top row) and of species 2 (bottom row) for the set of parameters corresponding to configurations E, F, G, H and I. The parameters used for modelling ϕ_{12} are described in Table II and the varying values of R_{12}^- and R_{12}^+ are reported in Table III.

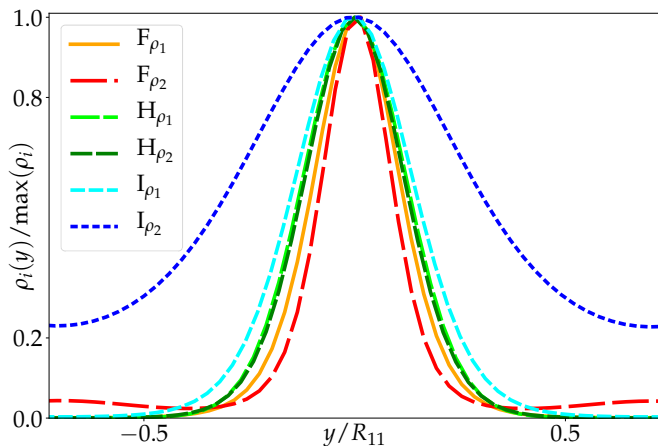


FIG. 5. One-dimensional density distributions $\rho_1(y)$ and $\rho_2(y)$ of a single condensation peak for cases F, H and I. The density is normalised by its maximal value. Minor peak size changes are found in ρ_1 for the different cases. However, ρ_2 peaks change significantly. In case F, species 2 occupies mainly the center of the particle. In case H, the two species are very well mixed. In case I, species 1 occupies the center of the aggregate.

matter such as core-shell structures and well-defined assemblies where the component species mix, yet granting control on mixing properties. We have identified the key intermolecular interactions features responsible for these complex self-assembling structures and demonstrated how the assembly and species mixing can be controlled. To this end, linear stability analysis was used a guiding principle.

This insight can be employed to better understand multi-component self-assembly systems that emerge in, e.g., cellular function and complex biological structure formation. It also paves the way for engineering advanced complex materials solutions for, e.g., drug delivery including anticancer therapy approaches that often rely on

sequential delivery of multiple drugs, see e.g. [80, 81].

In this work, we applied DFT to two different cases. First, we mapped out a rich phase diagram where one species occupies the core of the self-assembled particles and the second species surrounds the latter either as a freely solvated species or a corona layer depending on the concentrations of the two components. This assembly response, described in Sec. III, can be considered to correspond to spontaneous formation of droplets (for example, biomolecular condensation), polymer core-shell particles or surfactant micelles. Such systems are ubiquitous in biological systems but also chemical engineering such as paints, cosmetics, and pharmaceutical formulations.

We also demonstrated that via the effective interactions between the species, it is possible to carefully control not only the size of the self-assembling particles but also their internal composition gradient and mixing of the species inside the particles. Furthermore, the findings give access to controlling overall density distribution. These findings are summarized in Sec. IV. A handle to self-assembling particle internal composition has applications in molecular partitioning (hydrophobicity gradients), diffusion control, chemical reactions engineering but also in controlling solubilization and dispersion.

We note that the present theory is not restricted to (ultra) soft interaction potentials that were the main focus in this work. In fact, using different approximations for the free energy functionals, the theory developed here can be applied to a wide range of systems, including, e.g., colloids and nanoparticles. Additionally, one should note that the theoretical approach presented here can also be applied to systems exhibiting multiple length scales in their self-assembled configurations [46]. Examples of such systems that constitute coexisting structures with different length scales include, e.g., multi-core micelles [82–87], coacervate droplets in biocondensates (liquid-liquid phase-separation in biological systems) [88] and multiple emulsions [32].

VI. ACKNOWLEDGMENT

This work was supported by Academy of Finland grants No. 309324 (M.S.) and Nos. 307806 and 312298 (T.A.-N.). T.A.-N. has also been supported by a Technology Industries of Finland Centennial Foundation TT2020 grant. We are grateful for the support by FinnCERES Materials Bioeconomy Ecosystem. Computational resources by CSC IT Centre for Finland and RAMI – RawMatters Finland Infrastructure are also gratefully acknowledged.

VII. AUTHOR CONTRIBUTIONS

A.S. conceived the work, executed the theoretical calculations and wrote the first draft of the manuscript. M.S. and T.A.-N. supervised the research. All authors contributed to writing.

Appendix A: Asymmetry in capsule-like structures

The asymmetries in the equilibrium densities reported in Fig. 1 result from the relatively strong and long-ranged repulsion between particles of species 2 that compete with all other energy contributions in the system. This asymmetry can be diminished by reducing the integrated

strength of ϕ_{22} . This can be done by changing either the strength or the range of ϕ_{22} , i.e. by decreasing $\beta\epsilon_{22}$ or R_{22} (or both). To demonstrate this, we keep the repulsion strength between particles of species 2 at $\beta\epsilon_{22} = 1$, but change the range of the interaction by setting $R_{22} = 0.24$. Fig. 6 presents a comparison of the the density distribution of species 2 corresponding to $R_{22} = 0.24$ (panel V) and $R_{22} = 1$ (panel W). Panel W corresponds to the case reported in panel D $_{\rho_2}$ of Fig. 1.

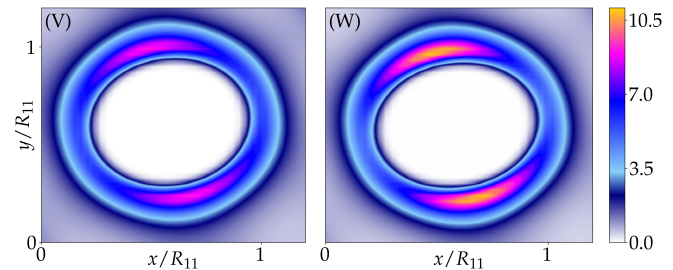


FIG. 6. Asymmetry dependence on R_{22} interaction parameter. Panel V shows $\rho_2(\mathbf{r})$ for $R_{22} = 0.24$ and panel W for $R_{22} = 1$. All other parameters are the same as in case D of Fig. 1. The asymmetry in the density distribution is visibly higher in panel W which corresponds to a longer-ranged ϕ_{22} . The maximal density value in W is roughly 20 % higher than in V.

-
- [1] G. M. Whitesides and M. Boncheva, “Beyond molecules: Self-assembly of mesoscopic and macroscopic components,” *Proceedings of the National Academy of Sciences*, vol. 99, no. 8, pp. 4769–4774, 2002.
 - [2] L. Wang, A. M. Urbas, and Q. Li, “Nature-inspired emerging chiral liquid crystal nanostructures: From molecular self-assembly to dna mesophase and nanocolloids,” *Advanced Materials*, vol. 32, no. 41, p. 1801335, 2020.
 - [3] G. R. Desiraju and G. W. Parshall, “Crystal engineering: the design of organic solids,” *Materials Science Monographs*, vol. 54, 1989.
 - [4] D. F. Evans and H. Wennerström, *The Colloidal Domain: Where Physics, Chemistry, Biology, and Technology Meet*. Wiley-VCH, second ed., 1999.
 - [5] M. N. Jones, D. Chapman, *et al.*, *Micelles, monolayers, and biomembranes*. Wiley-Liss, 1995.
 - [6] Y. Lu, J. Lin, L. Wang, L. Zhang, and C. Cai, “Self-assembly of copolymer micelles: Higher-level assembly for constructing hierarchical structure,” *Chemical Reviews*, vol. 120, no. 9, pp. 4111–4140, 2020.
 - [7] H. Hu, M. Gopinadhan, and C. O. Osuji, “Directed self-assembly of block copolymers: a tutorial review of strategies for enabling nanotechnology with soft matter,” *Soft Matter*, vol. 10, no. 22, pp. 3867–3889, 2014.
 - [8] M. A. Cohen Stuart, W. T. Huck, J. Genzer, M. Müller, C. Ober, M. Stamm, G. B. Sukhorukov, I. Szleifer, V. V. Tsukruk, M. Urban, *et al.*, “Emerging applications of stimuli-responsive polymer materials,” *Nature Materials*, vol. 9, no. 2, pp. 101–113, 2010.
 - [9] A. Kumar, N. L. Abbott, H. A. Biebuyck, E. Kim, and G. M. Whitesides, “Patterned self-assembled monolayers and meso-scale phenomena,” *Accounts of Chemical Research*, vol. 28, no. 5, pp. 219–226, 1995.
 - [10] R. K. Smith, P. A. Lewis, and P. S. Weiss, “Patterning self-assembled monolayers,” *Progress in Surface Science*, vol. 75, no. 1, pp. 1–68, 2004.
 - [11] R. Lifshitz and H. Diamant, “Soft quasicrystals—why are they stable?,” *Philosophical Magazine*, vol. 87, no. 18-21, pp. 3021–3030, 2007.
 - [12] S. F. Banani, H. O. Lee, A. A. Hyman, and M. K. Rosen, “Biomolecular condensates: organizers of cellular biochemistry,” *Nature Reviews Molecular Cell Biology*, vol. 18, no. 5, pp. 285–298, 2017.
 - [13] E. Sezgin, I. Levental, S. Mayor, and C. Eggeling, “The mystery of membrane organization: composition, regulation and roles of lipid rafts,” *Nature Reviews Molecular Cell Biology*, vol. 18, pp. 361–374, 06 2017.
 - [14] S. Yadav, A. K. Sharma, and P. Kumar, “Nanoscale self-assembly for therapeutic delivery,” *Frontiers in Bioengineering and Biotechnology*, vol. 8, p. 127, 2020.
 - [15] M. C. Branco and J. P. Schneider, “Self-assembling materials for therapeutic delivery,” *Acta Biomaterialia*, vol. 5, no. 3, pp. 817–831, 2009.
 - [16] K. Kataoka, A. Harada, and Y. Nagasaki, “Block copolymer micelles for drug delivery: design, characterization

- and biological significance,” *Advanced Drug Delivery Reviews*, vol. 64, pp. 37–48, 2012.
- [17] Z. Huang, W. Song, and X. Chen, “Supramolecular self-assembled nanostructures for cancer immunotherapy,” *Frontiers in Chemistry*, vol. 8, p. 380, 2020.
- [18] C. Oerlemans, W. Bult, M. Bos, G. Storm, J. F. W. Nijssen, and W. E. Hennink, “Polymeric micelles in anticancer therapy: targeting, imaging and triggered release,” *Pharmaceutical Research*, vol. 27, no. 12, pp. 2569–2589, 2010.
- [19] L.-L. Ma, W. Hu, Z.-G. Zheng, S.-B. Wu, P. Chen, Q. Li, and Y.-Q. Lu, “Light-activated liquid crystalline hierarchical architecture toward photonics,” *Advanced Optical Materials*, vol. 7, no. 16, p. 1900393, 2019.
- [20] F. Yang, S. Cheng, X. Zhang, X. Ren, R. Li, H. Dong, and W. Hu, “2d organic materials for optoelectronic applications,” *Advanced Materials*, vol. 30, no. 2, p. 1702415, 2018.
- [21] H. Shaikh, J. D. Garcia-Hernandez, M. Vespa, and T. Fukui, “Functional nanoparticles through pi-conjugated polymer self-assembly,” *Nature Reviews*, vol. 6, no. 1, pp. 7–26, 2021.
- [22] C. Yuan, X. Zhang, L. Su, B. Gao, and L. Shen, “Facile synthesis and self-assembly of hierarchical porous nano/micro spherical superstructures for high performance supercapacitors,” *Journal of Materials Chemistry*, vol. 19, no. 32, pp. 5772–5777, 2009.
- [23] J. G. Lyons, M. A. Plantz, W. K. Hsu, E. L. Hsu, and S. Minardi, “Nanostructured biomaterials for bone regeneration,” *Frontiers in Bioengineering and Biotechnology*, vol. 8, 2020.
- [24] S. Zhang, D. M. Marini, W. Hwang, and S. Santoso, “Design of nanostructured biological materials through self-assembly of peptides and proteins,” *Current Opinion in Chemical Biology*, vol. 6, no. 6, pp. 865–871, 2002.
- [25] R. Nagarajan and E. Ruckenstein, “Theory of surfactant self-assembly: a predictive molecular thermodynamic approach,” *Langmuir*, vol. 7, no. 12, pp. 2934–2969, 1991.
- [26] K. Birdi and S, *Handbook of surface and colloid chemistry*. CRC press, fourth ed., 2015.
- [27] T. F. Tadros, *Emulsions: Formation, stability, industrial applications*. Walter de Gruyter GmbH & Co KG, first ed., 2016.
- [28] J.-P. Hansen and I. R. McDonald, eds., *Theory of Simple Liquids*. Oxford: Academic Press, fourth ed., 2013.
- [29] R. Evans, “The nature of the liquid-vapour interface and other topics in the statistical mechanics of non-uniform, classical fluids,” *Advances in Physics*, vol. 28, no. 2, pp. 143–200, 1979.
- [30] J. F. Lutsko, “Recent developments in classical density functional theory,” *Advances in Chemical Physics*, vol. 144, p. 1, 2010.
- [31] A. Sorrenti, O. Illa, and R. M. Ortuño, “Amphiphiles in aqueous solution: well beyond a soap bubble,” *Chemical Society Reviews*, vol. 42, pp. 8200–8219, 2013.
- [32] T. Sheth, S. Seshadri, T. Prileszky, and M. E. Helgeson, “Multiple nanoemulsions,” *Nature Reviews Materials*, vol. 5, no. 3, pp. 214–228, 2020.
- [33] W. I. Mortada, “Recent developments and applications of cloud point extraction: A critical review,” *Microchemical Journal*, vol. 157, p. 105055, 2020.
- [34] S. De Koker, R. Hoogenboom, and B. G. De Geest, “Polymeric multilayer capsules for drug delivery,” *Chemical Society Reviews*, vol. 41, no. 7, pp. 2867–2884, 2012.
- [35] R. Ghosh Chaudhuri and S. Paria, “Core/shell nanoparticles: classes, properties, synthesis mechanisms, characterization, and applications,” *Chemical Reviews*, vol. 112, no. 4, pp. 2373–2433, 2012.
- [36] R. Haag, “Supramolecular drug-delivery systems based on polymeric core-shell architectures,” *Angewandte Chemie International Edition*, vol. 43, no. 3, pp. 278–282, 2004.
- [37] Y. Kakizawa and K. Kataoka, “Block copolymer micelles for delivery of gene and related compounds,” *Advanced Drug Delivery Reviews*, vol. 54, no. 2, pp. 203–222, 2002.
- [38] T. Trantidou, M. Friddin, Y. Elani, N. J. Brooks, R. V. Law, J. M. Seddon, and O. Ces, “Engineering compartmentalized biomimetic micro- and nanocontainers,” *ACS Nano*, vol. 11, no. 7, pp. 6549–6565, 2017.
- [39] H. Che and J. C. M. van Hest, “Stimuli-responsive polymersomes and nanoreactors,” *Journal of Materials Chemistry B*, vol. 4, pp. 4632–4647, 2016.
- [40] M. York-Duran, M. Godoy-Gallardo, C. Labay, A. Urquhart, T. Andresen, and L. Hosta-Rigau, “Recent advances in compartmentalized synthetic architectures as drug carriers, cell mimics and artificial organelles,” *Colloids and Surfaces B: Biointerfaces*, vol. 152, pp. 199 – 213, 2017.
- [41] J. Gaitzsch, X. Huang, and B. Voit, “Engineering functional polymer capsules toward smart nanoreactors,” *Chemical Reviews*, vol. 116, no. 3, pp. 1053–1093, 2016.
- [42] W. Somerville, J. Stokes, A. Adawi, T. Horozov, A. J. Archer, and D. Buzza, “Density functional theory for the crystallization of two-dimensional dipolar colloidal alloys,” *Journal of Physics: Condensed Matter*, vol. 30, no. 40, p. 405102, 2018.
- [43] D. Ratliff, A. Archer, P. Subramanian, and A. Rucklidge, “Which wave numbers determine the thermodynamic stability of soft matter quasicrystals?,” *Physical Review Letters*, vol. 123, no. 14, p. 148004, 2019.
- [44] A. Scacchi, W. Somerville, D. Buzza, and A. Archer, “Quasicrystal formation in binary soft matter mixtures,” *Physical Review Research*, vol. 2, no. 3, p. 032043, 2020.
- [45] P. Subramanian, D. J. Ratliff, A. M. Rucklidge, and A. J. Archer, “The density distribution in soft matter crystals and quasicrystals,” *arXiv preprint arXiv:2010.10191*, 2020.
- [46] A. Scacchi, S. J. Nikkhah, M. Sammalkorpi, and T. AlaNissila, “Self-assembly in soft matter with multiple length scales,” *arXiv preprint arXiv:2101.02468*, 2021.
- [47] A. J. Archer, M. J. Robbins, U. Thiele, and E. Knobloch, “Solidification fronts in supercooled liquids: How rapid fronts can lead to disordered glassy solids,” *Physical Review E*, vol. 86, no. 3, p. 031603, 2012.
- [48] A. J. Archer, M. C. Walters, U. Thiele, and E. Knobloch, “Solidification in soft-core fluids: Disordered solids from fast solidification fronts,” *Physical Review E*, vol. 90, no. 4, p. 042404, 2014.
- [49] A. J. Archer, M. C. Walters, U. Thiele, and E. Knobloch, “Generation of defects and disorder from deeply quenching a liquid to form a solid,” in *Mathematical Challenges in a New Phase of Materials Science* (Y. Nishiura and M. Kotani, eds.), (Tokyo), pp. 1–26, Springer Japan, 2016.
- [50] A. J. Archer, M. C. Walters, U. Thiele, and E. Knobloch, “Solidification in soft-core fluids: Disordered solids from fast solidification fronts,” *Physical Review E*, vol. 90, no. 4, p. 042404, 2014.

- [51] M. C. Walters, P. Subramanian, A. J. Archer, and R. Evans, "Structural crossover in a model fluid exhibiting two length scales: repercussions for quasicrystal formation," *Physical Review E*, vol. 98, no. 1, p. 012606, 2018.
- [52] A. Scacchi, A. J. Archer, and J. M. Brader, "Dynamical density functional theory analysis of the laning instability in sheared soft matter," *Physical Review E*, vol. 96, no. 6, p. 062616, 2017.
- [53] A. Scacchi, M. G. Mazza, and A. J. Archer, "Sensitive dependence on molecular interactions of length scales in sheared soft matter," *Physical Review Research*, vol. 2, no. 3, p. 032064, 2020.
- [54] T. V. Ramakrishnan and M. Yussouff, "First-principles order-parameter theory of freezing," *Physical Review B*, vol. 19, no. 5, p. 2775, 1979.
- [55] C. N. Likos, "Effective interactions in soft condensed matter physics," *Physics Reports*, vol. 348, no. 4, pp. 267–439, 2001.
- [56] A. Louis, P. Bolhuis, and J. Hansen, "Mean-field fluid behavior of the gaussian core model," *Physical Review E*, vol. 62, no. 6, p. 7961, 2000.
- [57] C. Likos, A. Lang, M. Watzlawek, and H. Löwen, "Criterion for determining clustering versus reentrant melting behavior for bounded interaction potentials," *Physical Review E*, vol. 63, no. 3, p. 031206, 2001.
- [58] A. Archer, C. Likos, and R. Evans, "Binary star-polymer solutions: bulk and interfacial properties," *Journal of Physics: Condensed Matter*, vol. 14, no. 46, p. 12031, 2002.
- [59] A. J. Archer, A. M. Rucklidge, and E. Knobloch, "Soft-core particles freezing to form a quasicrystal and a crystal-liquid phase," *Physical Review E*, vol. 92, no. 1, p. 012324, 2015.
- [60] H. M. Al-Saedi, A. J. Archer, and J. Ward, "Dynamical density-functional-theory-based modeling of tissue dynamics: application to tumor growth," *Physical Review E*, vol. 98, no. 2, p. 022407, 2018.
- [61] D. Coslovich, M. Bernabei, and A. J. Moreno, "Cluster glasses of ultrasoft particles," *Journal of Chemical Physics*, vol. 137, no. 18, p. 184904, 2012.
- [62] A. J. Archer and A. Maliyevský, "Crystallization of soft matter under confinement at interfaces and in wedges," *Journal of Physics: Condensed Matter*, vol. 28, no. 24, p. 244017, 2016.
- [63] A. Scacchi and J. M. Brader, "Flow induced crystallisation of penetrable particles," *Journal of Physics: Condensed Matter*, vol. 30, no. 9, p. 095102, 2018.
- [64] L. Caprini, E. Hernández-García, C. López, and U. M. B. Marconi, "A comparative study between two models of active cluster crystals," *Scientific Reports*, vol. 9, no. 1, pp. 1–13, 2019.
- [65] I. Götze, A. J. Archer, and C. Likos, "Structure, phase behavior, and inhomogeneous fluid properties of binary dendrimer mixtures," *The Journal of chemical physics*, vol. 124, no. 8, p. 084901, 2006.
- [66] S. Overduin and C. Likos, "Phase behaviour in binary mixtures of ultrasoft repulsive particles," *Europhysics Letters*, vol. 85, no. 2, p. 26003, 2009.
- [67] S. D. Overduin and C. N. Likos, "Clustering in nondemixing mixtures of repulsive particles," *Journal of chemical physics*, vol. 131, no. 3, p. 034902, 2009.
- [68] M. Camargo, A. J. Moreno, and C. N. Likos, "Dynamics in binary cluster crystals," *Journal of Statistical Mechanics: Theory and Experiment*, vol. 2010, no. 10, p. P10015, 2010.
- [69] M. Camargo and C. N. Likos, "Interfacial and wetting behaviour of phase-separating ultrasoft mixtures," *Molecular Physics*, vol. 109, no. 7-10, pp. 1121–1132, 2011.
- [70] C. N. Likos, B. M. Mladek, D. Gottwald, and G. Kahl, "Why do ultrasoft repulsive particles cluster and crystallize? analytical results from density-functional theory," *Journal of Chemical Physics*, vol. 126, no. 22, p. 224502, 2007.
- [71] P. Bolhuis, A. Louis, J. Hansen, and E. Meijer, "Accurate effective pair potentials for polymer solutions," *Journal of Chemical Physics*, vol. 114, no. 9, pp. 4296–4311, 2001.
- [72] C. Likos, H. Löwen, M. Watzlawek, B. Abbas, O. Jucknischke, J. Allgaier, and D. Richter, "Star polymers viewed as ultrasoft colloidal particles," *Physical Review Letters*, vol. 80, no. 20, p. 4450, 1998.
- [73] A. Louis, P. Bolhuis, J. Hansen, and E. Meijer, "Can polymer coils be modeled as "soft colloids"?, " *Physical Review Letters*, vol. 85, no. 12, p. 2522, 2000.
- [74] I. Götze, H. Harreis, and C. Likos, "Tunable effective interactions between dendritic macromolecules," *Journal of Chemical Physics*, vol. 120, no. 16, pp. 7761–7771, 2004.
- [75] C. N. Likos, "Soft matter with soft particles," *Soft Matter*, vol. 2, no. 6, pp. 478–498, 2006.
- [76] D. A. Lenz, R. Blaak, C. N. Likos, and B. M. Mladek, "Microscopically resolved simulations prove the existence of soft cluster crystals," *Physical Review Letters*, vol. 109, no. 22, p. 228301, 2012.
- [77] B. M. Mladek, D. Gottwald, G. Kahl, M. Neumann, and C. N. Likos, "Formation of polymorphic cluster phases for a class of models of purely repulsive soft spheres," *Physical Review Letters*, vol. 96, no. 4, p. 045701, 2006.
- [78] K. Zhang, P. Charbonneau, B. M. Mladek, *et al.*, "Reentrant and isostructural transitions in a cluster-crystal former," *Physical Review Letters*, vol. 105, no. 24, p. 245701, 2010.
- [79] N. B. Wilding and P. Sollich, "Demixing cascades in cluster crystals," *Journal of Chemical Physics*, vol. 141, no. 9, p. 094903, 2014.
- [80] M. S. Aw, M. Kurian, and D. Losic, "Polymeric micelles for multidrug delivery and combination therapy," *Chemistry - A European Journal*, vol. 19, no. 38, pp. 12586–12601, 2013.
- [81] M. Wu, Y. Zhu, and W. Jiang, "Disassembly of multi-compartment polymer micelles in spatial sequence using an electrostatic field and its application for release in chronological order," *Angewandte Chemie International Edition*, vol. 57, no. 14, pp. 3578–3582, 2018.
- [82] L. Wang and J. Lin, "Discovering multicore micelles: insights into the self-assembly of linear abc terpolymers in midblock-selective solvents," *Soft Matter*, vol. 7, no. 7, pp. 3383–3391, 2011.
- [83] H. Chen and E. Ruckenstein, "Formation and degradation of multicomponent multicore micelles: insights from dissipative particle dynamics simulations," *Langmuir*, vol. 29, no. 18, pp. 5428–5434, 2013.
- [84] N. Duxin, F. Liu, H. Vali, and A. Eisenberg, "Cadmium sulphide quantum dots in morphologically tunable triblock copolymer aggregates," *Journal of the American Chemical Society*, vol. 127, no. 28, pp. 10063–10069, 2005.

- [85] Z. Iatridi and C. Tsitsilianis, “pH responsive self assemblies from an a_n-core-(b-b-c)_n heteroarm star block terpolymer bearing oppositely charged segments,” *Chemical Communications*, vol. 47, no. 19, pp. 5560–5562, 2011.
- [86] M. Ueda, A. Hashizume, and T. Sato, “Unicore-multicore transition of the micelle formed by an amphiphilic alternating copolymer in aqueous media by changing molecular weight,” *Macromolecules*, vol. 44, no. 8, pp. 2970–2977, 2011.
- [87] H. Chen and E. Ruckenstein, “Formation of complex colloidal particles: morphologies and mechanisms,” *Soft Matter*, vol. 8, no. 34, pp. 8911–8916, 2012.
- [88] T. Lu and E. Spruijt, “Multiphase complex coacervate droplets,” *Journal of the American Chemical Society*, vol. 142, no. 6, pp. 2905–2914, 2020.